NIST-GCR-92-609

Soot Formation in the Buoyancy-Dominated Ethene Diffusion Flame

Haran Subramaniasivam

NIST

United States Department of Commerce
Technology Administration
National Institute of Standards and Technology

Soot Formation in the Buoyancy-Dominated Ethene Diffusion Flame

Haran Subramaniasivam

Brown University
Division of Engineering
Providence, RI 02912

Soot Formation In The Buoyancy-Dominated Ethene Diffusion Flame

by

Haran Subramaniasivam

B.S. Mechanical Engineering

Massachusetts Institute of Technology, Cambridge, **MA**

May, 1989

Thesis

Submitted in partial fulfillment of the requirements for the Degree of Master of Science in the Division of Engineering **at** Brown University

May, 1991

Acknowledgements

I would like to express my gratitude first and foremost to my research advisor, Professor Richard A. Dobbins, for his guidance and supervision over the past two years.

I would also like to express my gratitude to Mr. Allan Schwartzman, Research Engineer in charge of the Electron Microscope Facility, and to Professor Steven R. Nutt for instruction in the use of the Philips TEM. Mr. William Lilly has provided invaluable technical assistance with data acquisition and equipment modification.

This thesis by Haran Subramaniasivam is accepted

in its present form by the Department of Engineering as satisfying

the thesis requirement for the degree of Master of Science

Date ....
                                                   Professor Richard A. Dobbins

Approved by the Graduate Council

Date ....
                                                   Dean Phillip J. Stiles

TABLE OF CONTENTS

LIST OF FIGURES

ABSTRACT

A sampling technique, based on the phenomenon of thermophoresis is used here, in order to study the soot morphology within **a** buoyancy-dominated ethene diffusion flame. The buoyancy-dominated flame **has** a fuel flow rate of 50 cc/s and a co-annular air flow of 107 cc/s. Soot morphologies at each sampling location are obtained on carbon-coated grids through a fast probe drive mechanism, and they are analyzed under a transmission electron microscope. These observations, coupled with temperature measurements at various heights of the buoyancy-dominated flame, leads to **a** basic understanding of particle inception region, surface growth, aggregate formation, oxidation process, aggregate size and primary particle size within this flame. Change in soot morphology is studied both in the vertical and radial **axes** of this flame. The intense particle inception region, characterized by a large concentration of liquid-like microdroplets, is contained within the low part of the flame. These microdroplets form on the fuel side of the flame front where the temperature is the highest. Above the inception region aggregates of increasing size are observed, i.e., increasing number of primary particles, while the primary particles themselves undergo surface growth. Surface growth in primary particles ceases to exist above the vortex region of the flame, i.e., above $Z=15$ cm. Since there is very little evidence of oxidation taking place within this buoyancy-dominated flame, it **is** concluded that most of the soot formed in this flame is released into the surroundings. Observations being made here have been compared to similar soot morphology studies previously made on laminar ethene diffusion flames, both non-sooting and sooting, and laser diagnostic tests.

I. INTRODUCTION

The knowledge of controlling combustion, carrying out fire research, the ability to convert chemical energy with greater efficiency and reduce health hazards are some of the incentives for studying formation, transport, oxidation and emission of soot in flames. To this end non-intrusive laser light scattering and transmission analyses of flames have been widely performed[1-3] . Yet these analyses fail to completely explore the dynamic processes that take place in a flame, especially in the soot inception region near the burner mouth. The need to understand the morphological features of soot formation lead to the improvement of the intrusive thermophoretic sampling technique4 . Thermophoresis is the drift of **a** particle down a temperature gradient. The testing method is designed to reduce contamination of the sample collection grids by regions of high soot concentration, and also possesses moderate spatial resolution with respect to flame coordinates. These thermophoretic samples are subsequently analyzed by transmission electron microscopy. In the recent past this testing method has been widely used by Megaridis and Dobbins in their studies of soot formation in laminar ethene diffusion flames[5-7] . The goal of the present research project **is** to **map** the soot morphology in **a** buoyancy-dominated flame which **is** representative of many flames in fires. Limited studies have been performed on turbulent and buoyancy-dominated diffusion flames[8,9] but little effort has been

1

devoted to understanding soot formation in these flames. Other long standing and disputes on the presence of nucleation and growth of soot particles exist[10]. Further detailed studies of chemical species and soot particle concentration have been carried out with good spatial resolution on laminar diffusion flames[11].

This study describes the initial observations of soot formation in a buoyancy-dominated ethene diffusion flame. The 13 hertz oscillation observed low in this flame amplifies into an irregular vortex structure at approximately 15 cm above the burner. The top of the flame exhibits strongly unsteady flickering. In this work, the soot morphology in this flame has been explored in various regions of the flame. Transmission electron microscopy leads to **a** better understanding of primary particle sizes, and the process of surface growth and aggregation of primary soot particles within **a** flame. **A** successful effort has been made to determine regions of soot inception, surface growth, aggregation, oxidation and soot release to the atmosphere. Findings have been compared to similar analyses performed on laminar ethene diffusion flames[7]. Furthermore the above observations can be used to elucidate some unexplained findings in certain regions of the flame obtained through laser light scattering and extinction tests. Combined with previous findings these results provide valuable information on the structure of both the buoyancy-dominated and the laminar ethene diffusion flames.

Thermophoretic sampling technique discussed here complements the optical analysis method by providing morphological information that

is necessary for the data reduction of the optical experiment. The use of both these methods leads to **a** more complete understanding of soot formation process in flames.

II. __EXPERIMENTAL__

Thermophoretic sampling technique and the probe attachments are described here followed by discussions of the probe control system and the burner arrangement. **A** brief description of the flame structure and the modus operandi of the experiment concludes this chapter.

Thermophoresis, the phenomenon of a particle travelling down a temperature gradient, is created here by introducing **a** cold-surface inside a particle-laden flame. The cold-surface, i.e. probe, will initially be at room temperature. The probe exposure time **has** to be long enough for soot particles to deposit on it yet should be sufficiently brief **so** that it remains **a** cold surface, as required for thermophoresis. The probe consists of carbon-coated grids on which soot sample is deposited. Therefore the exposure time has an upper bound determined by the stability of these grids upon exposure to high temperatures within the flame. The cold probe surface will tend to freeze any heterogeneous reactions of the deposited particles, providing yet another advantage in using the thermophoretic sampling technique. This sampling method has been extensively **used** to study soot in flames through transmission electron microscopy analysis[2,12-14] .

THERMOPHORETIC PROBE ATTACHMENTS:

The probe attachment consists of two components: the bulk specimen carrier and carbon-coated electron microscope grids. The bulk specimen carrier, made up of an alloy of copper, nickel and zinc, has dimensions 11.5x3.0x0.15 mm. This carrier, more specifically designed for scanning electron microscopy (SEM) is produced by Philips Electronic Instruments, Inc., and is shown in Figure 1a. The bulk specimen carriers acquired from Philips are modified by machining a slit of about 10 mm long and 1.5 mm wide along it's center as shown in Figure 1b.

Electron microscope grids are disks of diameter 3.05 mm (Figure 1c.) consisting of a fine mesh with a thin carbon film coating. The carbon film has a low tolerance of exposure to flame temperatures. Figure 1d shows as to how the grids are attached to the modified bulk specimen carrier. A thin layer of Miller-Stephenson 907 two-part epoxy is spread on the bulk specimen carrier, and three grids are attached to it, as shown, covering approximately a 9 mm length of the carrier. For the given bulk specimen carrier-grid attachments, it was experimentally determined that at an exposure time in excess of 100 ms the grids began to oxidize and became useless. Typical experimental exposure times ranged between 70 and 100 ms.

Forceps with extremely fine tips are used in handling the bulk specimen carrier and the grids in order not to contaminate them. All

items mentioned here are stored in a desicator when not in use. Exposed bulk specimen carriers, under such careful storage, show no evidence of deterioration over as long **a** period as one month. Yet, whenever possible, fresh bulk specimen carrier-grid attachments are prepared immediately prior to each test run.

PNEUMATIC PROBE CONTROL SYSTEM:

Very short probe insertion **and** retraction times are needed when compared to the probe's residence time within the flame. Such an action reduces contamination of the grids. Contamination of the grids occurs when a section of a grid, attached to **a** bulk specimen carrier, passes through a region in the flame of high soot particle concentration before reaching the desired flame location to be sampled. **To** this end a securely mounted double-acting pneumatic piston is used as the mechanical actuator of the probe control device. The pneumatic source is nitrogen gas and the operational pressure **is** approximately 450 kPa absolute. Insertion and retraction times are approximately 12 ms each. Though typically about 70 ms **is** used, this arrangement has the ability to produce residence times **as** low **as** 30 ms. The probe trajectory **is** observed on an oscilloscope. Such **a** trace **is** been reproduced in Figure 2.

This pneumatic probe device could be moved both horizontally and vertically, potentially enabling every location of the flame to be inspected and analyzed. These motions are carried out radially and vertically to within three-tenths of a millimeter. The

reproducibility of the probe trajectory and it's alignment with respect to flame coordinates are very good.

Previous studies, using high-speed photography, by Dobbins and Megaridis[4] have shown that sudden insertion of the probe causes severe distortion of the smaller laminar diffusion flame.   Such a distortion makes spatial resolution along flame coordinates impossible.   The buoyancy-dominated unsteady flame has a larger fuel flow rate than the laminar flame, therefore it is less prone to distort when the probe is suddenly inserted into it radially.   In order to safeguard against such a distortion of the flame coordinates a shield, shown in Figure **4,** was designed and installed. **As** evidenced through high-speed photography, this modification lead to remarkable improvement in the probe insertion technique thereby giving the aforementioned high spatial resolution.

A fully assembled bulk specimen carrier-grid arrangement, prepared **as** described before, is then attached to the probe before insertion into the flame.   The probe and the carrier are then moved closer to the flame for insertion.   At such close proximity to the flame the bulk specimen carrier and the grids could be potentially exposed to somewhat elevated temperatures for **a** significant time.   In order to protect the delicate grids and keep them at room temperature **a** nitrogen flow **is** passed over the probe and the bulk specimen carrier-grid attachment.   Just before the probe **is** inserted into the flame this nitrogen flow is completely shut off.   Then the probe is fired into the flame and retracted.   Previous studies have shown that

7

this nitrogen flow has no bearing on the flame or probe position. Repeated experiments over the past five years have shown that it's operation is remarkably reproducible and very accurate.

BURNER AND FLAME BEHAVIOR:

The photograph Figure 3a shows a typical ethene diffusion flame as seen by the eye. This photograph is obtained at a 1/15th of a second exposure time (see appendix for additional details on photographs). A schematic of this flame is shown in Figure 3b for the purpose of illustrating the four vertical sampling locations discussed in this thesis. A typical flame temperature measured by a 25 micrometer platinium/platinium-rhodium thermocouple at Z=1, as a function of radial coordinate R, is shown in Figure 3c.

The burner is designed to support a co-annular diffusion flame. As shown in Figure 4 the brass burner fuel supply tube is 11.1 mm in diameter and is surrounded by an outer brass tube of diameter 101.6 mm. Compressed dry air with maximum moisture of 3 ppm is fed to the flame through the region between the inner and outer tubes. An arrangement of 3 mm glass beads, distributor plates and air chamber at the bottom of the burner provide a uniform air flow. This burner set up has been extensively used in previous laser scattering and transmission measurements on co-annular diffusion flames[3,15] .

A typical buoyancy-dominated co-annular ethene diffusion flame, supported by a fuel flow of 50 cc/sec and air flow of 107 cc/sec, is approximately 40 cm high. The Reynolds number of the flame at the

8

burner mouth **is** approximately 400.   Due to the flickering nature of the upper flame it is not possible to accurately measure the flame height.   **As** shown in Figure 3 the lower end of the flame was composed of a nearly laminar structure, therefore the diameter of the flame **is** approximately that of the burner mouth.   Flame front, the region of highest temperature, **is** clearly evident **as** it is the brightest region when radially traversing the flame at any given vertical location.   **A** few burner diameters above the burner mouth, approximately 2=5 cm, the flame begins to show evidence of oscillations at a frequency close to 13 hertz as observed by others8 . **Also** approximately at this height the bright region bifurcates, one portion continuing along the flame front while the other part tapers in towards the center of the flame.   The flame front itself loses it's appearance of a laminar structure as it begins to expand radially outward at a vertical height of approximately five burner diameters. The flame shows a very turbulent structure, evidenced through large vortices, at a height of approximately 15 cm from the burner.   This pear-shaped region, shown in Figure 3,   is about *5* cm in diameter at it's widest and about 7 cm long.   The formation and shedding of these vortices **is** shown in Figures 5a, 5b, 5c and 5d, which are sequential and instantaneous high-speed photographs taken at **an** exposure time of 1/500th of **a** second.   Above this turbulent region the flame front again moves inwards towards the center of the flame.   At **a** height of about 30 cm above the burner mouth the flame loses it's structure and begins to flicker.   The upper end of the flame could be seen between the heights of Z=40 cm and Z=45 cm.   At this height soot can be seen by the eye being emitted from the flame.

TYPICAL EXPERIMENT:

The flame **is** being probed at various radial locations at the heights Z = 0.5, 1, **2, 5,** 11, 15, *25* and 33 cm. Each of these experiments were run at least three times.

Once the set of Z and R flame coordinates of the respective flame locations to be tested are determined, the probe device, consisting of the aforementioned bulk specimen carrier-grid attachment in place, is set to be actuated along appropriate flame coordinates with the maximum precision. Then the flame itself is allowed to burn, at an ethene flow of 50 cc/sec and eo-annular air flow of 107 cc/sec, for about 30 minutes in order to allow the burner to reach steady temperature. Precautions are taken so that the experimental rig sits in a well ventilated area with as little air currents flowing near the flame. The pneumatic probe, with compressed nitrogen gas as it's power source, is then actuated firing and retracting the probe device. The exposure times of the grids inside the flame is predetermined and set accordingly. The trajectory of the probe can be recorded, through a translational transducer, on a storage oscilloscope and photographed. While this is not carried out each time it **is** run, the trajectory of the probe is periodically checked to confirm it's accuracy. The insertion and retraction times are 12 ms each and the typical residence time varies between 70 and 100 **rns.**

The probe **is** fitted with a new bulk specimen carrier-grid attachment after each test and is realigned to a new set of flame

coordinates in order to carry out the next experiment. After each series of tests, the air and fuel flow are turned off at the source and the fuel line **is** purged with nitrogen gas in order to remove fuel gases.

The bulk specimen carrier-grid attachment that **was** used in the experiment **is** then inserted into **a** Philips 420 STEM microscope and analyzed. Typically magnification setting ranging between 24,000 and 105,000 are used on the STEM with an electron beam accelerating voltage of 120 kV.

III. DISCUSSION OF SOOT MORPHOLOGY

The sampling locations are noted by flame coordinates, therefore Z and R the vertical and radial coordinates respectively measured, in centimeters, from the center of the burner mouth, where **Z=O** cm and R=O cm.

CHANGE IN SOOT MORPHOLOGY ON THE VERTICAL 'Z' AXIZ:

Z=1 cm, R=O cm: Figure **6a** represents this location. The aforementioned 13 hertz flickering is not evident and here the flame has a laminar appearance. Polydispersed isolated particles of various diameters exist with largest *of* approximately 20 nm to the smallest of approximately 3 nm. There **is** reason to expect that much smaller particles exist at this flame location but the microscope resolution establishes the smallest observable particle size. An important observation **is** the ratio of primaries to young aggregates which is approximately 25 to 1. **Also** most of the single primaries form irregular discoid images on the micrograph. Furthermore the aggregates themselves are not composed of uniform discoids but rather appear to be a collection of irregular discoids seemingly glued together. This morphology **is** refered to **as** agglutination, and aggregates exhibiting this quality are considered as young aggregates. Aggregates of many sizes, i.e., number of primaries in an aggregate, are present at this location, some with only 2 primaries while some have as many as 40 primaries. Most of

12

the monomers at this location appear quite transparent to the electron beam, i.e. their image on the photograph appears less distinct and faint.

Z=5 cm, R=0 cm: This location **is** just before the flame bifurcates and is shown in Figure 6b. One of the most notable features at this location **is** the decrease in the ratio of primaries to aggregates to about 10 to 1. Here too isolated droplets as small **as** 3 nm are seen though some of these primaries appear more distinctly, i.e. less transparent to the electron beam, than at the lower height. The aggregates at this height show less agglutination and some are composed of primaries as large as 25 nm. Yet these aggregates show a composition of both large and somewhat smaller primaries. Aggregates of varying sizes, i.e., aggregates composed varying number of primary particles, can also be seen at this location.

Z=15 cm, R=0 cm: The middle of the aforementioned pear-shaped region that contains large vortices is shown in Figure 6c. In stark contrast to the previous two locations here no evidence of unagglomerated singlets exist. Almost all of the many micrographs obtained at this location do not show evidence of agglutinated particles forming aggregates. Otherwise most micrographs exhibit aggregates composed of as few as 20 primaries to some in excess of 200 primaries. Almost all primaries at this location are of uniform **size,** approximately 35 nm in diameter, and their images have regular discoid shapes with no signs of agglutination.

Z=33 cm, R=O cm: This location, shown in Figure 6d, indicates the start of the flickering region at the top of the flame. Most micrographs obtained at this height exhibit aggregates with primary size approximately equal to that observed at Z=15 cm, R=0 cm location. However, there are some micrographs that also exhibit a few aggregates composed exclusively of smaller primaries. There is no evidence of single primaries or agglutinated aggregates at this location. At all previous flame locations a probe exposure time of 70 ms was employed. A longer exposure time of approximately 100 ms **is** used at this location in order to capture **a** sufficient sample.

CHANGE IN SOOT MORPHOLOGY ON THE RADIAL 'R' AXIS:

The unsteadiness of the buoyancy-dominated flame can impede radial analysis on soot morphology with satisfactory spatial resolution throughout most of this flame. However this flame shows no evidence of unsteadiness at heights below Z=5 cm. This lead to the study of soot morphology in the radial direction at Z=1 cm. An effort **is also** made to corelate these observations to the temperature trend in the radial direction at this height. The radial analysis of soot morphology is carried out using the above mentioned bulk specimen carrier-grid attachment, and then using the multiple holder in the Philips 420 STEM microscope. This holder enables the bulk specimen carrier-grid attachment to be moved along its length under the electron beam, thereby giving a radial mapping of soot morphology at any given fixed Z. The precision in the radial direction **is** within 0.3 mm. The temperature trend is obtained with

14

a Pt/Pt-Rh thermocouple of 25 micrometer diameter and the data is recorded at a frequency of 10 Hz through computerized data acquisition system. The temperatures read from this thermocouple are not corrected for either conduction or radiational losses. Our goal is to observe the trend of the temperature as a function of R and relate it to the change in soot morphology.

Soot **Morphology:** Figure 7 a, **b,** c and d represent soot morphology at Z=1 cm and R=0.42, 0.56, 0.63 and 0.70 cm respectively. At R=0.42 both aggregates composed of small primary particles and transparent droplet-like discoids are seen. **As** shown in Figure 7a there are very few young aggregates when compared to the number of polydisperse isolated particles present at this location. Furthermore these aggregates exhibit an agglutinated appearance similar to that observed at Z=1 cm, R= 0 cm location. Figure 7b shows soot morphology at R=0.56 cm. Here too young agglutinated aggregates and polydisperse droplet-like particles are seen and the ratio between them is about 1 to 10. **At** R=0.63 cm, shown in Figure 7c, the ratio between these two specific soot morphologies reduces to about 1 to 2. R=0.70 cm shown in Figure 7d shows an approximate ratio of 3 to 1 between the young agglutinated aggregates and the transparent polydisperse droplets. It **is** observed that the flame front, therefore the location of highest flame temperature, at Z=1 cm is approximately at R=0.65 cm.

Temperature Profile: This shown in Figure 8 with temperature in the vertical axis in degrees Celsius and the radial location in the

15

horizontal axis in centimeters. Therefore R=0 cm corresponds to the center of the flame at Z=1 cm. The highest indicated temperature of approximately 1,700 degrees Celsius is observed at a radial location between R=0.6 cm and R=0.7 cm. At the center of the flame, therefore when R=O cm, the temperature is approximately 100 degrees Celsius. At any given fixed Z, diametrically opposed points along the radius should give approximately the same temperature value. But as it can be seen in figure 8 this is not the case. For example, at the two R=1.5 cm locations the indicated temperature values are approximately 50 and 200 degrees Celcius. This discrepancy is attributed inaccuracies induced on the thermocouple due to the warming of the protective ceramic insulator around it.

DISCUSSION OF RESULTS OF SURVEY IN THE ETHENE DIFFUSION FLAME:

These observations are significant in understanding the physical evolution of soot along the length of the buoyancy-dominated ethene diffusion flame. The existence of a large concentration of transparent droplets at the burner mouth and the reduction of this concentration at higher heights suggests that of an intense soot particle inception region between the heights Z=1 cm and Z=5 cm. The coexistence of agglutinated aggregates consisting of primaries larger than the nascent droplets suggest that monomers in this region go through surface growth while also forming young aggregates through monomer-monomer and monomer-cluster aggregation processes. Agglutinated appearance of young aggregates

16

in this region is attributed to viscous material bonding the primaries that compose an aggregate. Figure 10 of the morphology at Z=l cm and R=0.5 cm is a clear representation of the above observations. The reduction in transparent droplet and monomer concentration at higher heights is attributed to a diminishing inception rate and to depletion by collisional processes. The greater transparency to the electron beam shown by most of the monomers in this region lends credence to the belief that these singlets have not yet been graphitized, an annealing process that requires longer exposure to elevated temperatures within the flame. Conversely any primary particle that displays high contrast on the micrograph would be a well annealed particle. Consistent with this description, such annealed particles are observed at Z=5 cm in larger numbers than at location Z=1 cm. The observations discussed here are consistent with the hypothesis that the intense soot particle inception is confined to **a** region low in the flame. The region discussed above is shown as Zone I in Figure 9.

The region between heights Z=5 cm and Z=15 cm is shown as Zone II in Figure **9.** The absence of any transparent droplets in this region indicates that this location is beyond the soot inception region. The evidence of only a very few monomers when compared to aggregates suggests that extensive monomer-cluster aggregation takes place in this zone. The existence of larger aggregates, i.e. consisting of more primaries, proves that cluster-cluster aggregation **also** takes place in this region. The primaries observed in this region are somewhat monodisperse and are larger in diameter than those observed in Zone

I, supporting the existence of surface growth in Zone II. The longer residence time that soot particles **will** sustain in the vortices that are present at this height explains the rapid and extensive surface growth. **A** hypothesis of rapid ingestion of fuel from the core of the flame by the vortices might explain this rapid surface growth seen on primaries. The average monomer diameter of approximately 35 nm seen at $Z=15$ cm is the largest that has been observed in the entire flame. This suggests that little, if any, surface growth takes place beyond Zone II. In their studies of pre-mixed flames, Harris and Weiner concluded that surface growth stops not due to depletion of the species contributing to the surface growth of primary particles but rather by the depletion in reactivity of the particles themselves[18, 19].

Zone III in Figure 9 exists above the vortices. Here extremely large aggregates, some consisting in excess of 200 primaries, are seen in addition to smaller clusters. There **is** no evidence of isolated singlets in this region. This leads to the belief that soot in this region consists mainly of cluster-cluster aggregation only. **A** small number of aggregates were observed consisting exclusively of many smaller primaries particles. Their presence can be explained by either of two scenarios: (a) these unique aggregates went through smaller degree of surface growth in Zones I and II, or **(b)** these are fully developed aggregates that have gone through partial oxidation in the upper part of the flame. Furthermore the existence of aggregates in the flickering region at the top of the flame demonstrates that this buoyancy-dominated ethene diffusion flame

18

releases soot into the atmosphere as is apparent to the unaided eye. The oxidation of soot particles in this flame appears reduced and most of the soot formed in the lower flame is released to the atmosphere. **This** could explained through the temperature profile at Z=15 cm as shown in Figure 11, The maximum temperature observed in this graph is about 1100 K. Temperature profiles obtained at heights above Z=15 cm show temperature trends less than 1100 K. **As** explained by Glassman[20], particle burnout ceases at a temperature of approximately 1350 K. Even though the temperature values in Figure 11 have not been corrected for any losses, it reasonable to assume that they are less than 1350 K, and therefore offer a plausible explanation for lack of oxidation of the soot particles in this flame.

At Z=1 cm, when radially traversing the flame outward from the center, the concentration of single, transparent liquid drop-like particles increase till just inside the flame front and then rapidly diminish in concentration. Whereas the agglutinated young aggregates remain constant in concentration till just outside the flame front where they suddenly appear in a very large concentration. The electron microscope grids that record the radial locations inside the flame front have *to* travel through this region of high young aggregate concentration before reaching their desired sampling regions. This **is** the aforementioned source of probable contamination of the grids. This suggests that the aggregates found on the micrographs inside the flame front may result from contamination. This conclusion and the above radial soot morphology

observations suggest that regions of high concentration of transparent droplet-like discoids and young agglutinated aggregates exist just inside and outside the flame front respectively. It is also important to note that the region of highest flame temperature **is** situated between these two regions of high concentration. This **is** a confirmation of an observation made by others[3] showing that the number concentration of soot particles attains **a** minimum at the region of highest flame temperature.

The small isolated droplets formed low in the flame are liquid-like in that they are capable of undergoing the coagulation process wherein collisions result in coalescence. Alternatively, the isolated droplets may collide with young aggregates and contribute to its agglutinated structure. We adopt the term " microdroplet " to describe the nascent liquid-like particles. This term was initially used by Lahaye and Prado who argued for the presence of these microdroplets based on kinetic calculations employing the theory of homogeneous nucleation[16]. They described the " liquid microdroplets " as a precursor to carbon black. An earlier discussion of these ideas was by Sweitzer and Heller whose experiments lead them to conclude that **"...** the immediate precursor to the carbon black particle is **a** tiny oil droplet"[17].

Our observations can be interpreted in terms of the above comments. A high population of microdroplets **is** observed on the fuel side of the flame front (Figure 7b) where the fuel molecules and their pyrolysis products are in high concentration. In this region the

microdroplet inception and coagulation rates are high and produce a polydisperse population of singlet droplets. Towards the higher temperature region at the flame front, the inception rate is lower and collisions deplete the microdroplet concentration. **At** the **same** time higher temperature leads to the rapid annealing of the aggregates. Thus at $Z=1$ cm, $R=0.65$ cm, which represents the flame front where the temperature is maximum, one finds in Figure 7d, the near total dominance of the aggregate population. We conclude that our micrograph observations are consistent with the presence of the smaller more transparent singlet particles existing **as** a nascent, liquid-like microdroplet which **is a** condensation product and **is** the nongaseous precursor to the annealed soot particle.

COMPARISON TO LAMINAR ETHENE DIFFUSION FLAME:

In the laminar flame, with an ethene flow rate of approximately 3.85 cc/s, the flame height **h** is smaller than h_{smoke}, where h_{smoke} is the critical height for the flame to begin emitting smoke. Therefore all soot formed in the laminar ethene diffusion flame is completely oxidized. **A** comparable analysis, just as the one done on buoyancy-dominated flame in Figure 9, would include a Zone IV above Zone III where soot is completely oxidized, i.e., no soot is emitted into the surroundings. Taller laminar ethene diffusion flames, with a fuel flow rate of approximately 5.00 cc/s, have been observed to release a large fraction of the soot formed into the atmosphere, i.e., complete oxidation of soot particles does not take place in these flames. In comparison, in the buoyancy-dominated flame very little

21

oxidation takes place and therefore most soot formed **is** released into the surroundings.

IV. __CONCLUSION__

A thermophoretic sampling technique is used in order to study changes in soot morphology in a buoyancy-dominated ethene diffusion flame with a fuel flow rate of 50 cc/s and **a** co-annular air flow of 107 cc/s. This flame is approximately **40** cm high and shows strong evidence of flickering at the top. Transmission electron microscopy **is** used to analyze the soot morphology at various locations in the flame. Strong evidence of transparent liquid-like microdroplets along with agglutinated young aggregates low in the flame. Their presence indicates that the particle inception region is situated low in the flame till approximately $Z=5$ cm. The existence of young aggregates composed of a few primary particles indicates, that in addition to soot particle inception, this region also consists of surface growth, monomer-monomer aggregation and some monomer-cluster aggregation. Above this height and below the vortex structure situated at $Z=15$ cm, the aggregates become less agglutinated and the primary particles that compose these aggregates undergo surface growth. The aggregates also appear longer than in the inception region. Therefore this region consists surface growth, monomer-cluster aggregation and cluster-cluster aggregation. The primary particles in this region are the largest observed in this flame and their diameter is about 35 nm. Above this region the only noticeable change in soot morphology is the appearance of even longer aggregates indicating the existence of cluster-cluster aggregation till the top of the flame. The lack of

23

adequately high temperature, i.e., above 1350 K, above $Z=15$ cm, is attributed to the very little oxidation observed in this flame. Therefore almost all the soot observed at $Z=15$ cm in this flame **is** released into the surroundings. Radial analysis of this flame **is** limited to the lower part of the flame because of the oscillating nature of the flame. Radially at $Z=1$ cm, regions of high concentration of microdroplets and young aggregates **are** seen just inside and outside the flame front, which **is** the location of highest flame temperature at that height. This not only confirms the existence of the particle inception region low in the flame, but it also indicates that the inception region exists inside the flame front.

Soot morphology is very important in interpreting the data from the laser light scattering/extinction experiments. We show that low in the flame particles may exist **as** liquid-like microdroplets, or **as** young agglutinated aggregates, or as a combination of both these morphologies. The laser light scattering/extinction analysis cannot distinguish these disparate morphologies in the small size limit where the optical response **is** independent of shape. Thus a sphere and an aggregate of equal volume produce the same scattering and absorption in Rayleigh size limit. Clearly the optical data will be more difficult to interpret when **a** combination of microdroplets and young agglutinated aggregates are present.

Appendix A. PHOTOGRAPH AND NEGATIVE LOG:

Flame : Buoyancy-dominated ethene diffusion flame with a fuel flow of 50 cc/s and a co-annular air flow of 107 cc/s.

escription of Transmission Flectron Micrograph negatives:

Fiaure	Neaative #	escription		
6a	6051	$Z=1$,	$R=0$,	x24,000
6b	5300	$Z=11$, $R=0$,		x62,500
6c	5368	$Z=25$, $R=0$,		x86,000
6d	5375	$Z=33$, $R=0$,		x86,000
7a	6133	$Z=1$,	$R=0.36$,	x24,000
7b	6131	$Z=1$,	$R=0.50$,	x24,000
7c	6130	$Z=1$,	$R=0.57$,	x24,000
7d	6129	$Z=1$,	$R=0.64$,	x24,000
10	5293	$Z=1$,	$R=0.5$,	x62,500

Note: Z and R are in centimeters & x = magnification setting on the TEM.

Description of photographs:

Film: Ektar, ASA 1000

Fiaure	Neaative #	Description
1a	12A	et = 1/15, f = 22
5a	4A	et = 1/500, f = 8
5b	0A	et = 1/500, f = 8
5c	6A	et = 1/500, f = 8
5d	8A	et = 1/500, f = 8

Note: et = exposure time in seconds & f = aperture setting

REFRENCES:

1. D'Alessio, **A.,** Di Lorenzo, **A.,** Borghese, **A.,** Beretta, F. and Masi, **S.,** Sixteenth Symposium (International) on Combustion, The Combustion Institute, page 695 (1977).

2. Prado, G., Jagoda, J., Neoh, K. and Lahaye, J., Eighteenth · Symposium (International) on Combustion, The Combustion Institute, page 1127 (1981).

3. Santoro, R., Semerjian, H. and Dobbins, R., Combustion and Flame, page 203 (1983).

4. Dobbins, R. and Megaridis, C., LANGMUIR, 3, 254 (1987).

5. Megaridis, **C.** and Dobbins, **R.,** Sixtieth Colloid and Surface Science Symposium (1986).

6. Megaridis, C. and Dobbins, R., Twenty Second Symposium (International) on Combustion, The Combustion Institute, page 353 (1988).

7. Megaridis, C. and Dobbins, R., Combustion Science and Technology, 66, 1 (1989).

8. Becker, H. and Liang, D., Combustion and Flame, 52, 247 (1983).

9. **Davis, R.,** Moore, E., Roquemore, **W.,** Chen, L., Vilimpoc, **V.** and **Goss,** L., Combustion and Flame, 83, 263 (1991)

10. Lahaye, J., Prado, G. and Donnet, J., Carbon,12, 27 (1974).

11. Prado, G., Lee, M., Hites, R., Hoult, R. and Howard, J., Sixteenth Symposium (international) on Combustion, The Combustion Institute, page 649 (1977).

12. Tesner, P.,Snegiriova, T. and Knorre, V., Combustion and Flame,17, 253 (1971).

13. Jagoda, I., Prado, G. and Lahaye, J., Combustion and Flame, 37, 261 (1980).

14. Skolnik, E. and McHale, E., Combustion and Flame, 37, 327 (1980).

15. Santoro, R., Yeh, T. and Semerjian, H., Twenty Third ASME/AIChE National Heat Transfer Conference, 1985.

16. Lahaye, J. and Prado, G., Water, Air, and Soil Pollution, 3, 473 (1974).

17. Sweitzer, C. and Heller, G., Rubber World, page 855 (1956).

18. Harris, S. and Weiner, A., Combustion Science and Technology, 31, 155 (1983).

19. Harris, S. and Weiner, A., Twentieth Symposium (international) on Combustion, The Combustion institute, page 969 (1985).

20. Glassman, I., Twenty-Second Symposium (international) on Combustion, The Combustion Institute, page 295 (1988).

(a) bulk specimen carrier

(b) TEM grid

(c) modified bulk specimen carrier

(d) bulk specimen carrier with the grids attached

9 mm
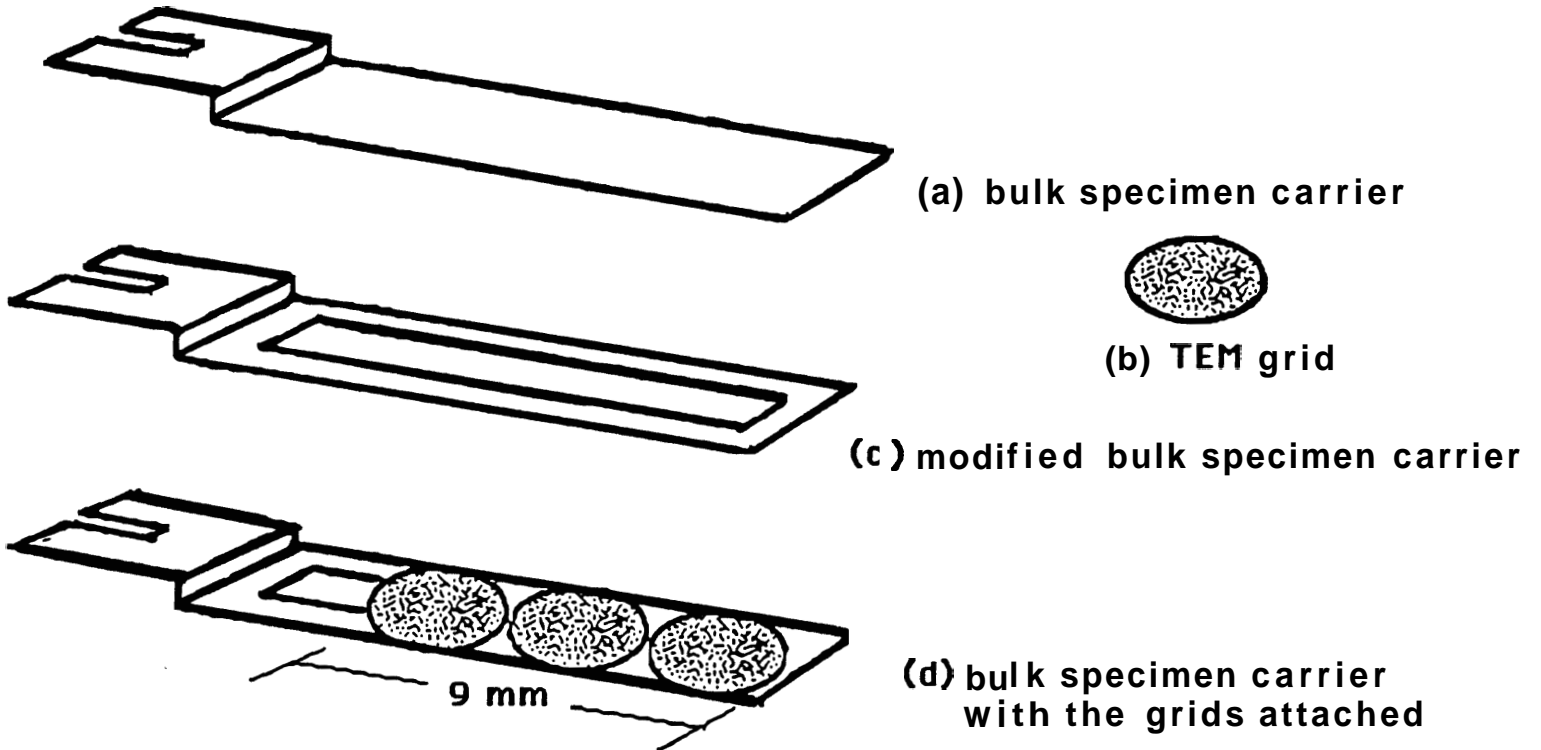
Figure 1: Bulk Specimen Carrier–Grid Attachment

t_e = 70 ms

t_t = 10 ms

t_t = 10 ms

displacement

time
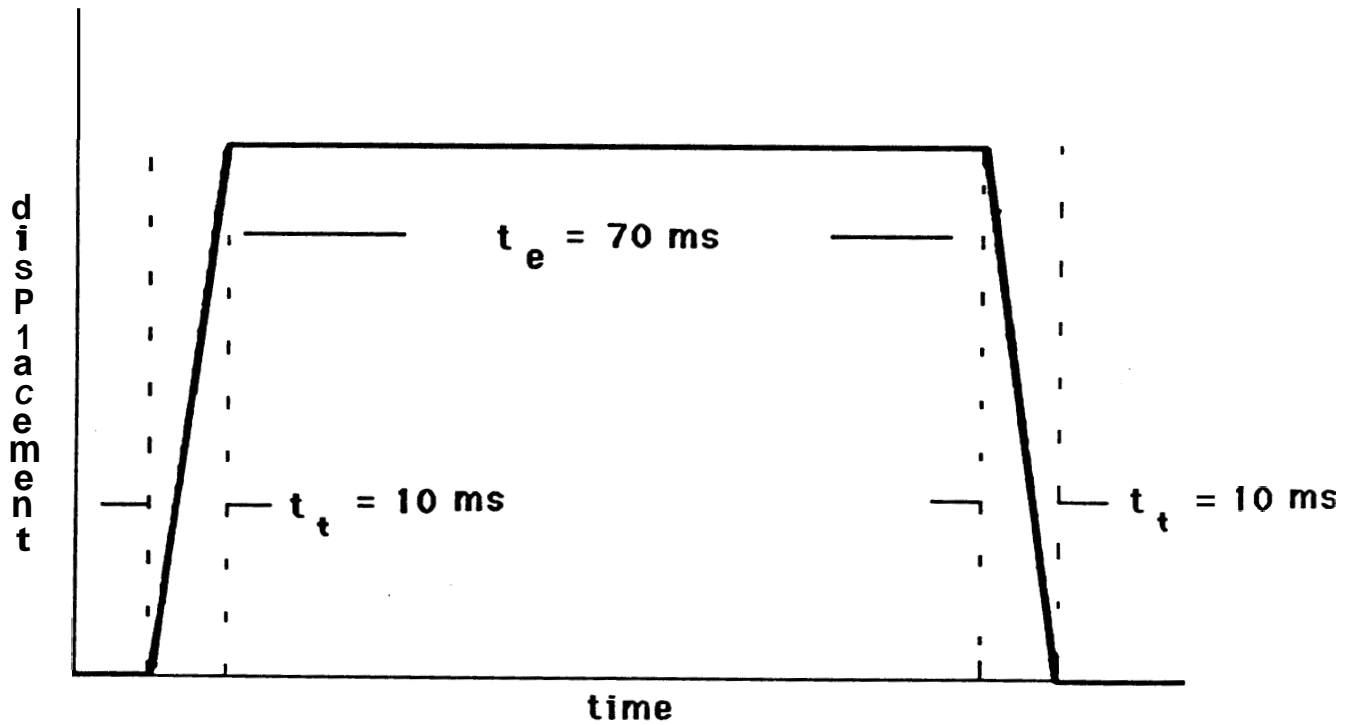
Figure 2: Probe trajectory

28
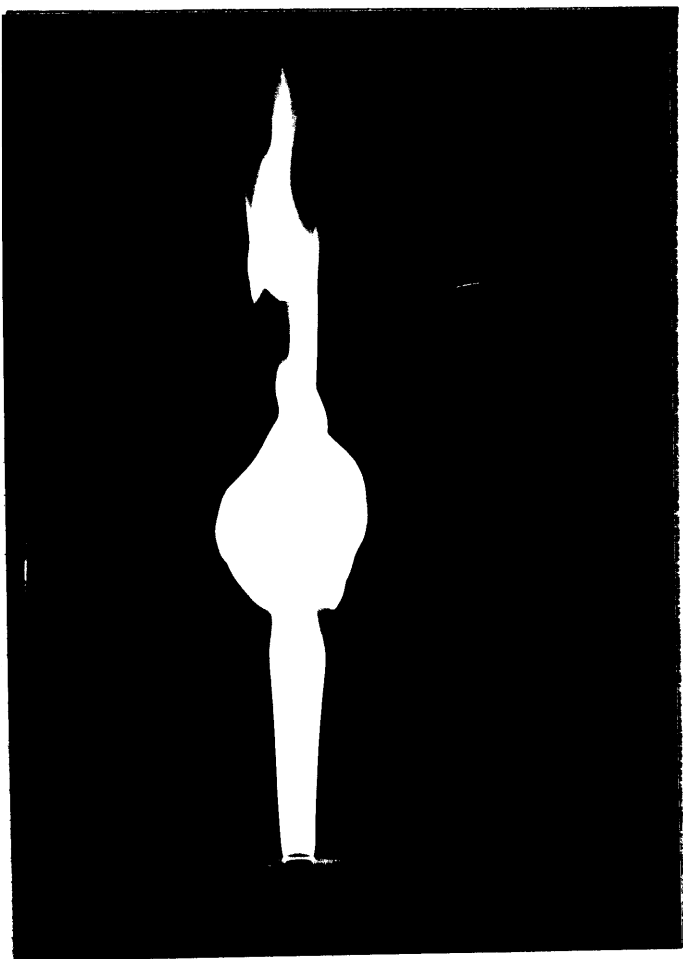
(a) Ethene buoyancy-dominated flame as seen by the eye

(b) Schematic of the buoyancy-dominated flame
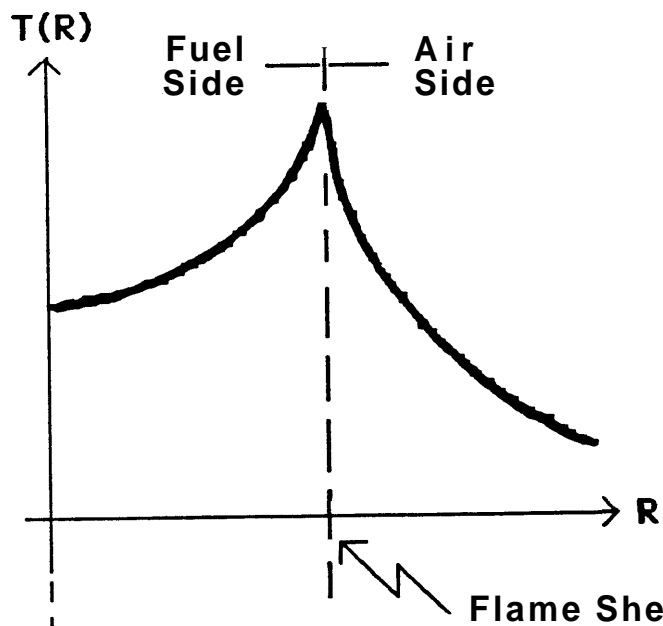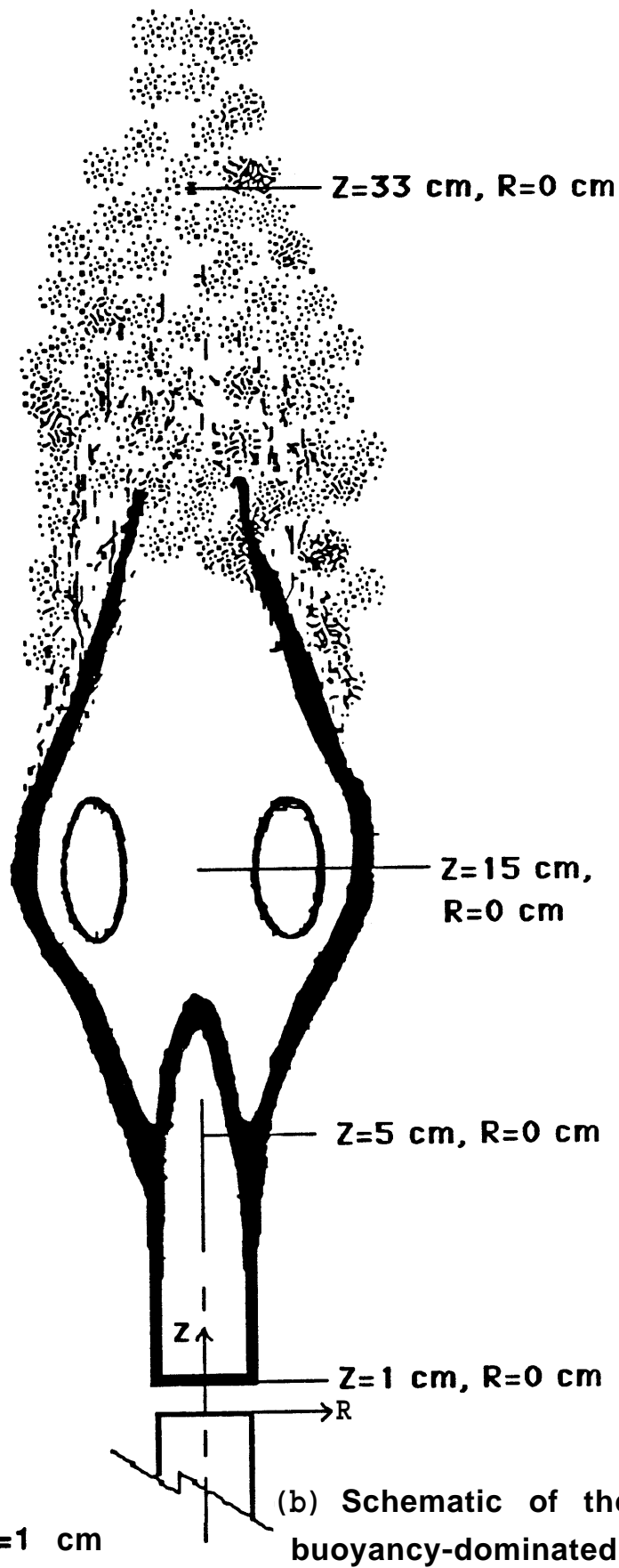
(c). Typical temperature profile at Z=1 cm

Figure 3: Schematic Diagram of the Buoyancy–Dominated Ethene Diffusion Flame with flame Coordinates

29
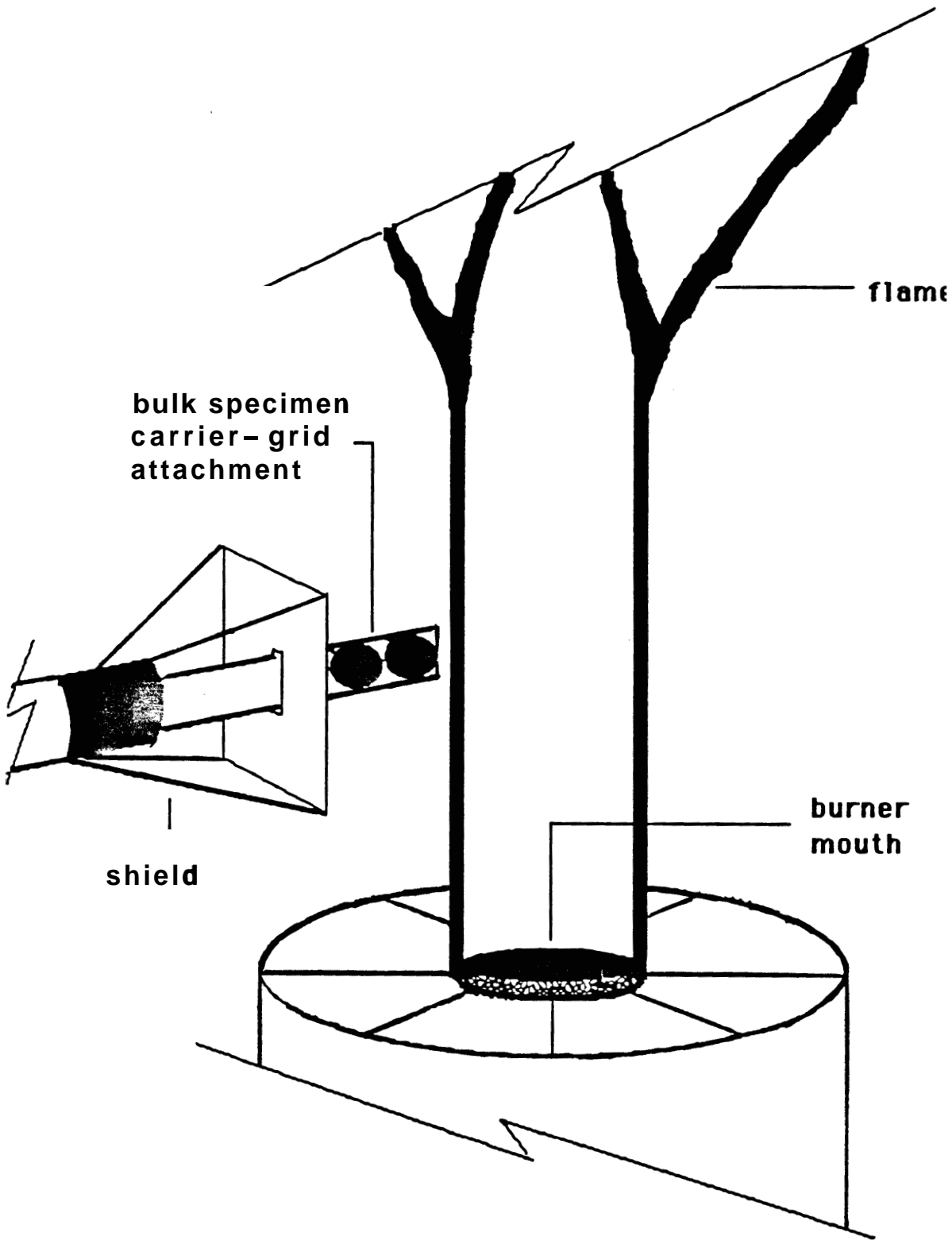
Figure 4: Burner and Shield Arrangement
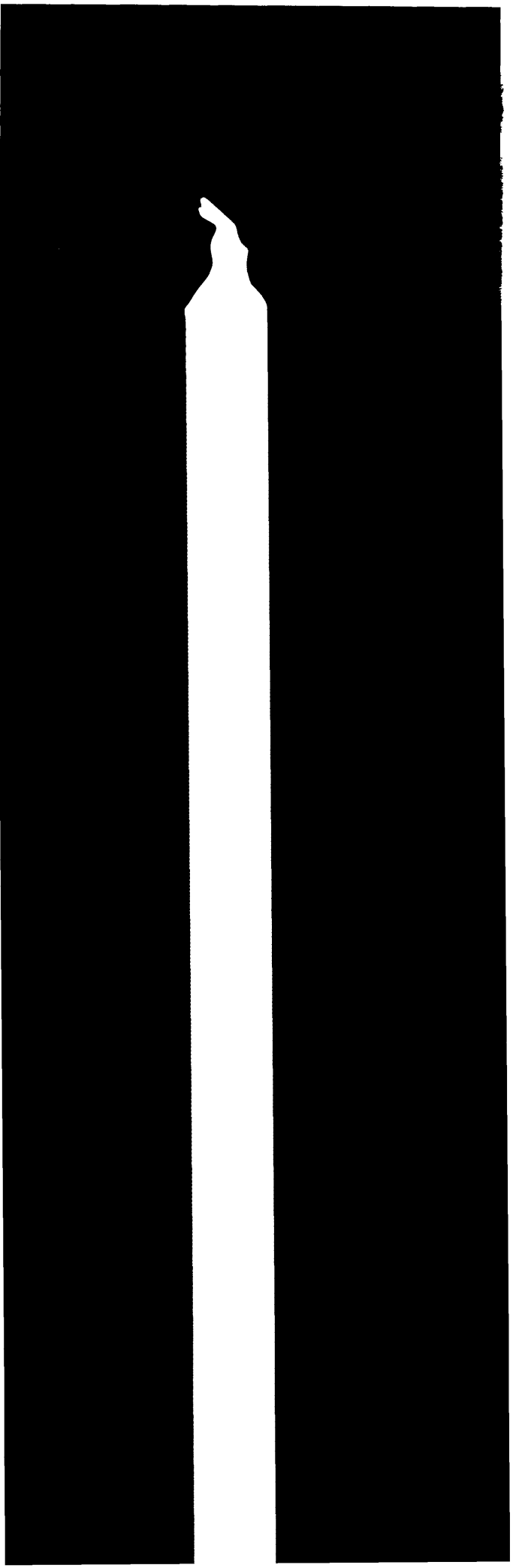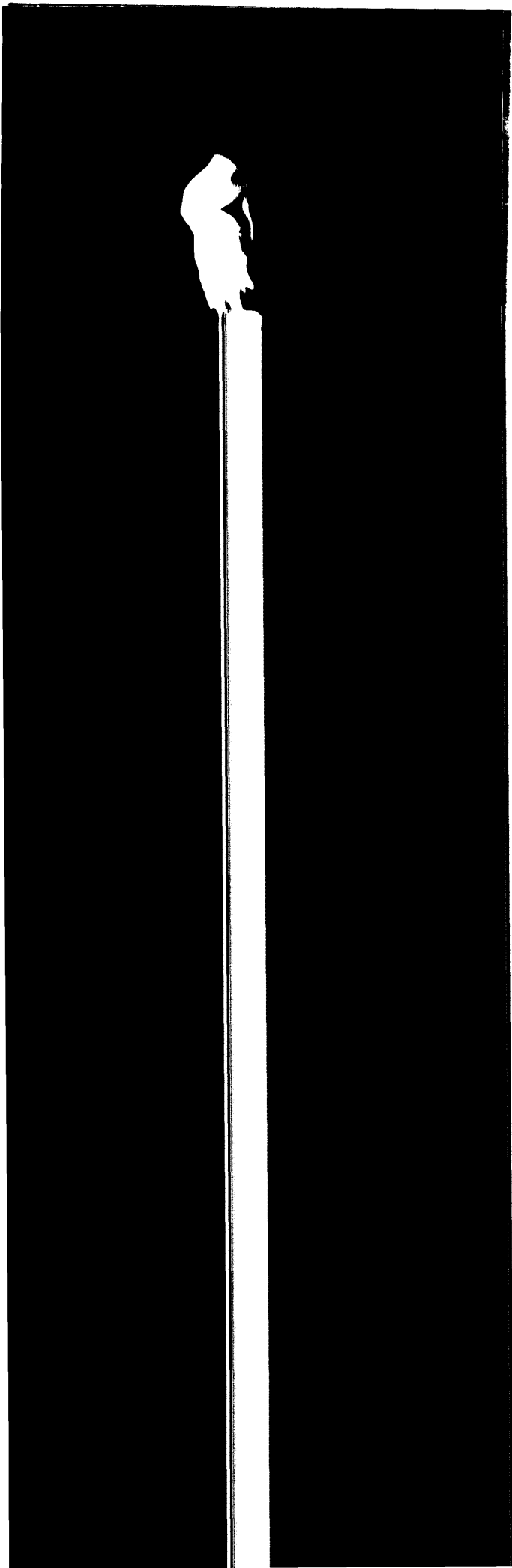
(a)
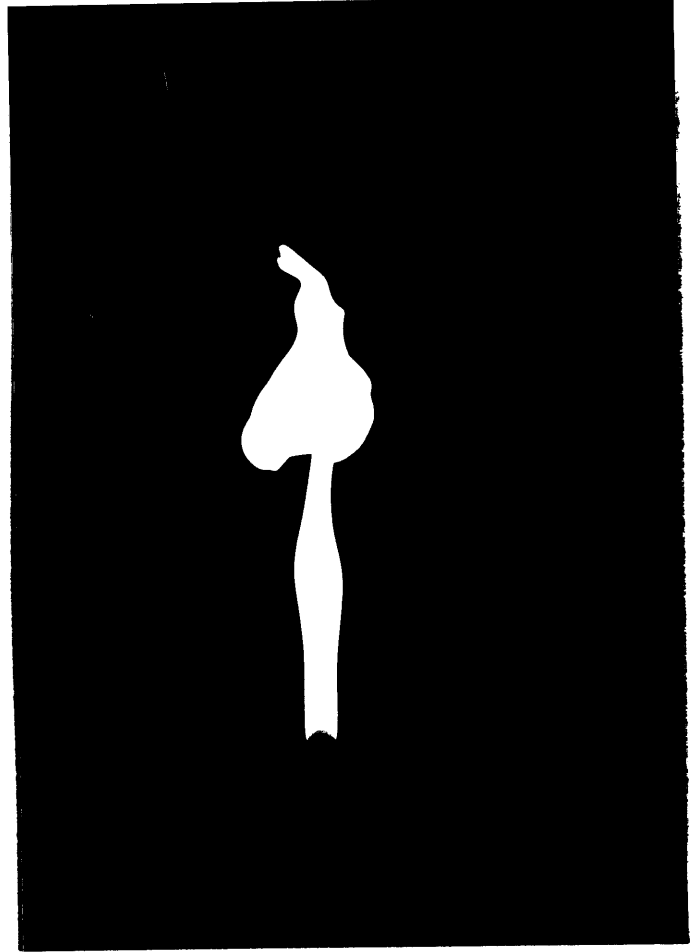
(b)

(c)
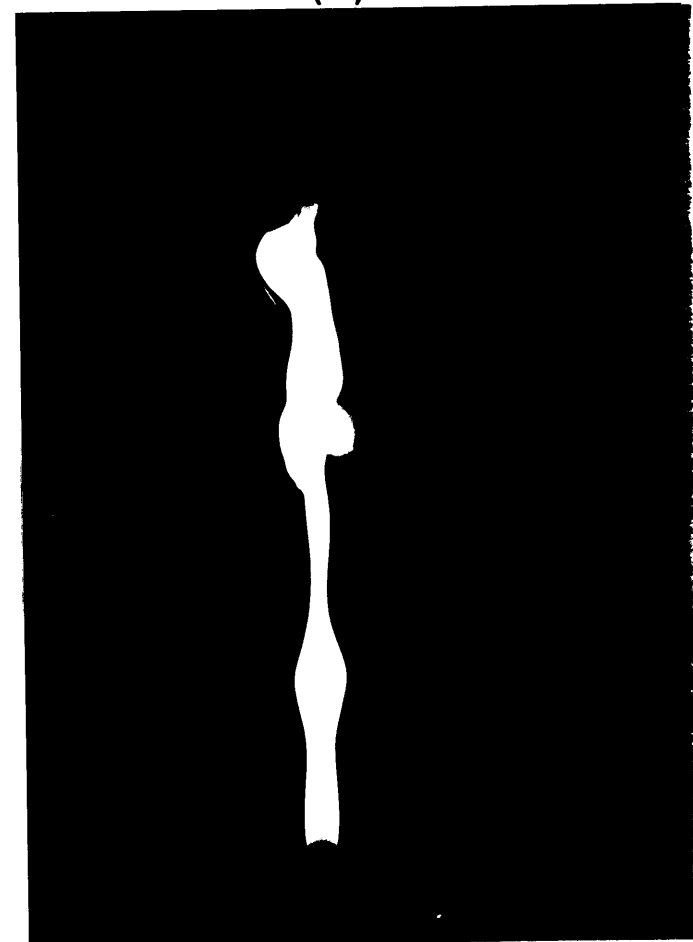
(d)

Figure 5: Illustration of Vortex Formation and Shedding
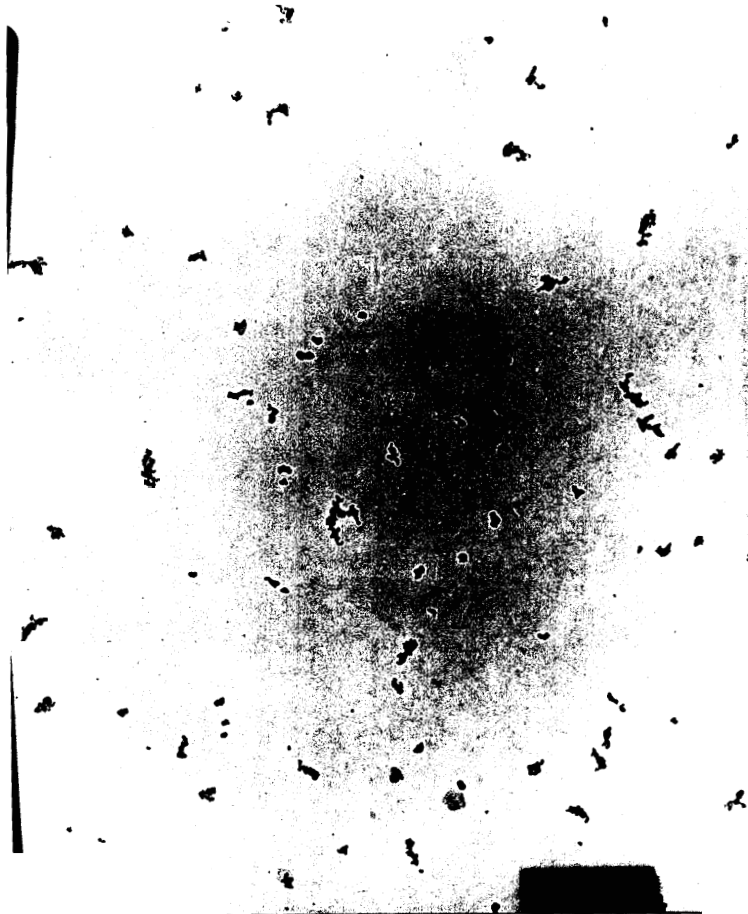
(a) Z=1 cm, R=O cm

(b) Z=11 cm, R=0 cm

(c) Z=25 cm, R=0 cm

(d) Z=33 cm, R=0 cm

Figure 6: Change in Soot Morphology in the Vertical 'Z' Axis

32
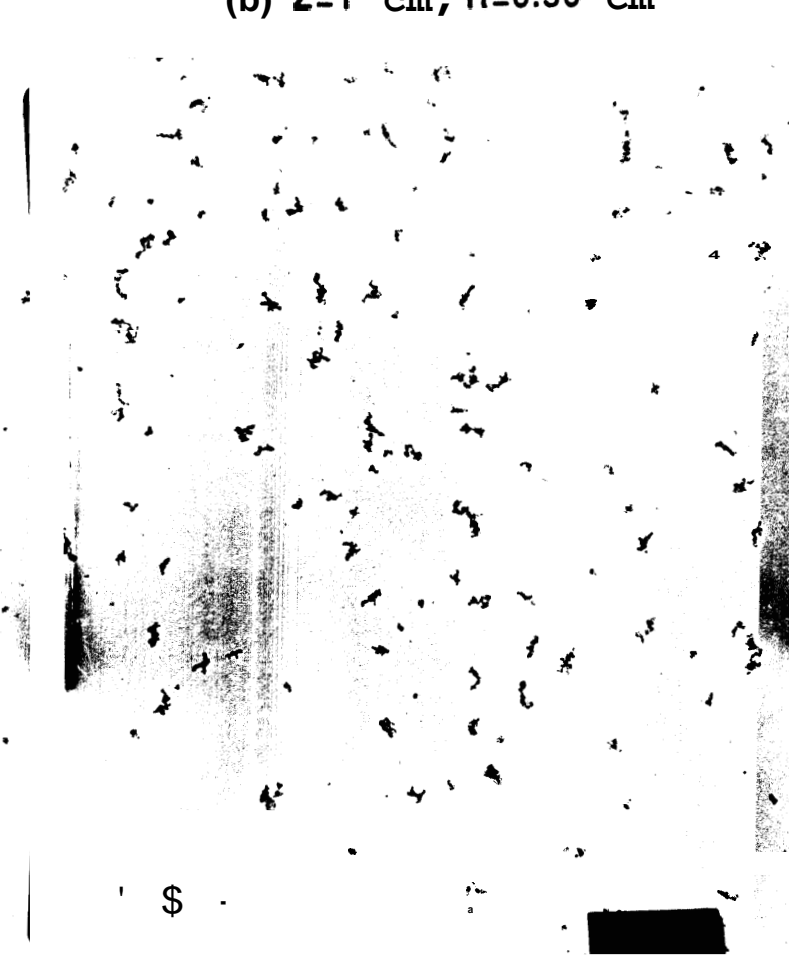
(a) Z=1 cm, R=0.36 cm

(b) Z=1 cm, R=0.50 cm

(c) Z=1 cm, R=0.57 cm

(d) Z=1 cm, R=0.64 cm

Figure 7: Change in Soot Morphology in the Horizontal 'R' Axis

Flame Map:CCF1.Z01

°C

2000

°C

7.1   5.5   3.9   2.3   .7   .7   2.3   3.9   5.5   7.1
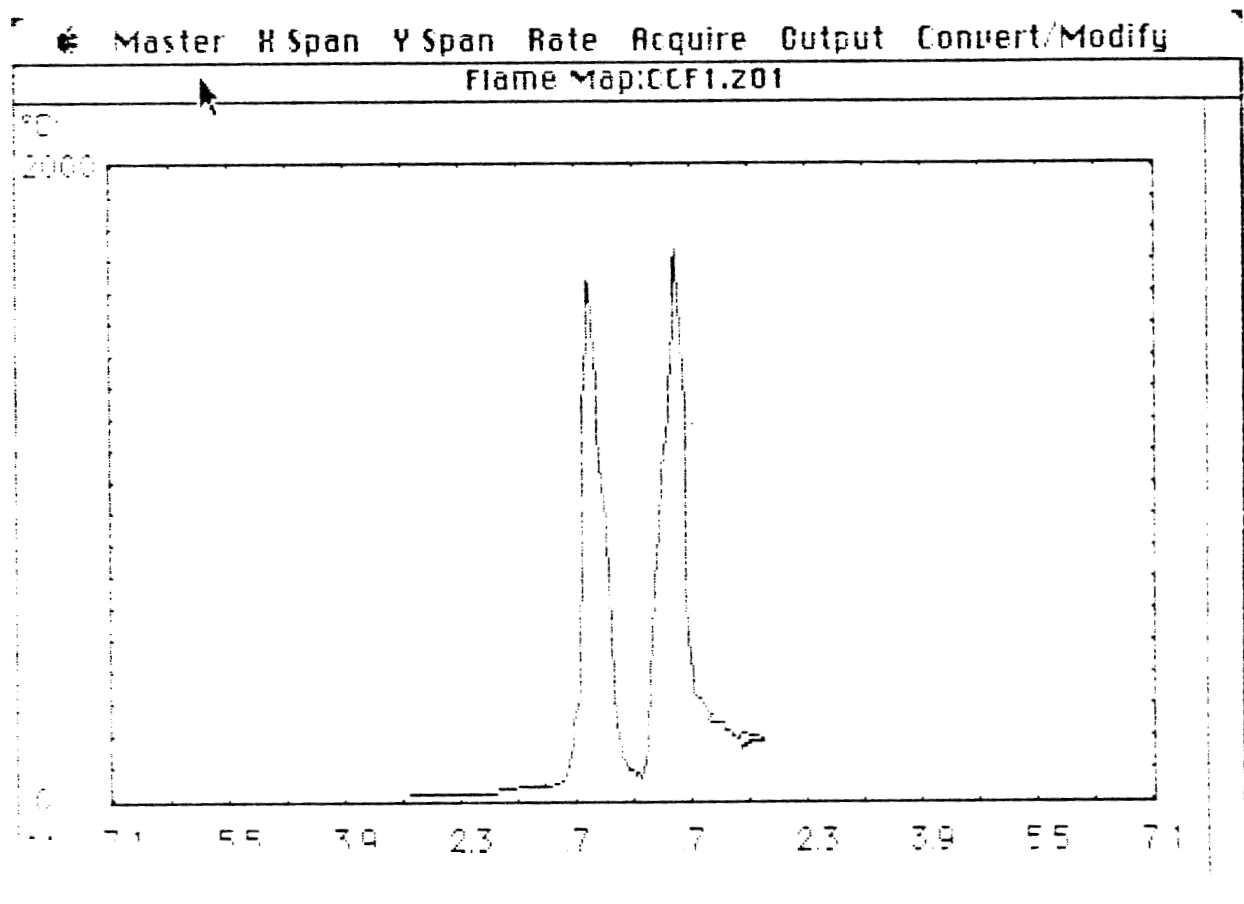
Figure 8: Temperature profile, T vs R, at Z=1 cm

34

Zone III
Soot Release

Z=3 cm, R=O cm

Zone II
Soot Growth

Z=15 cm

Z=5 cm, R=O cm

Zone I
Soot Inception &
Early Growth

Z=1 cm, R=O cm
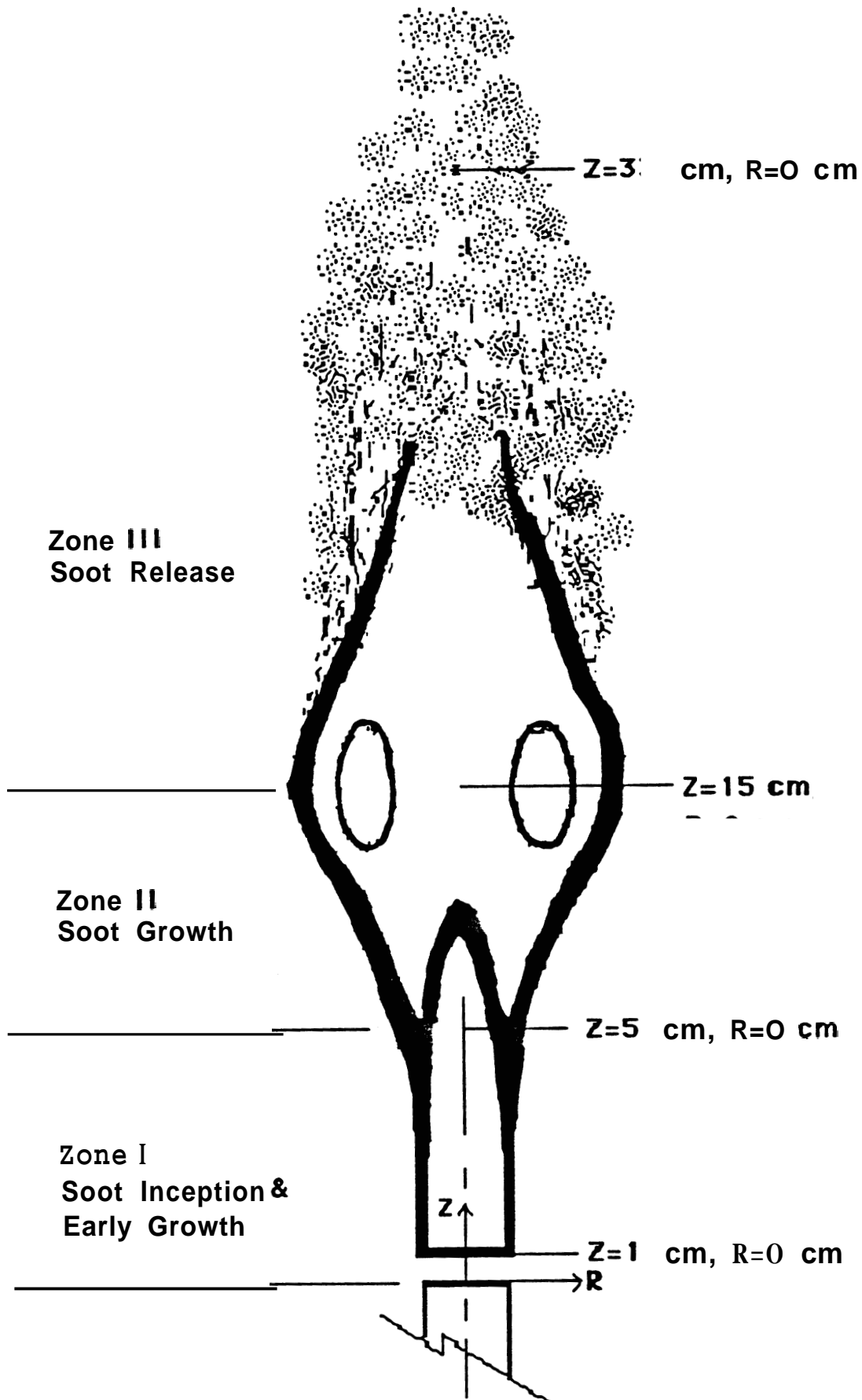
Figure 9: Schematic of the Buoyancy-Dominated
Flame Partitioned into Zones I, II & III

35
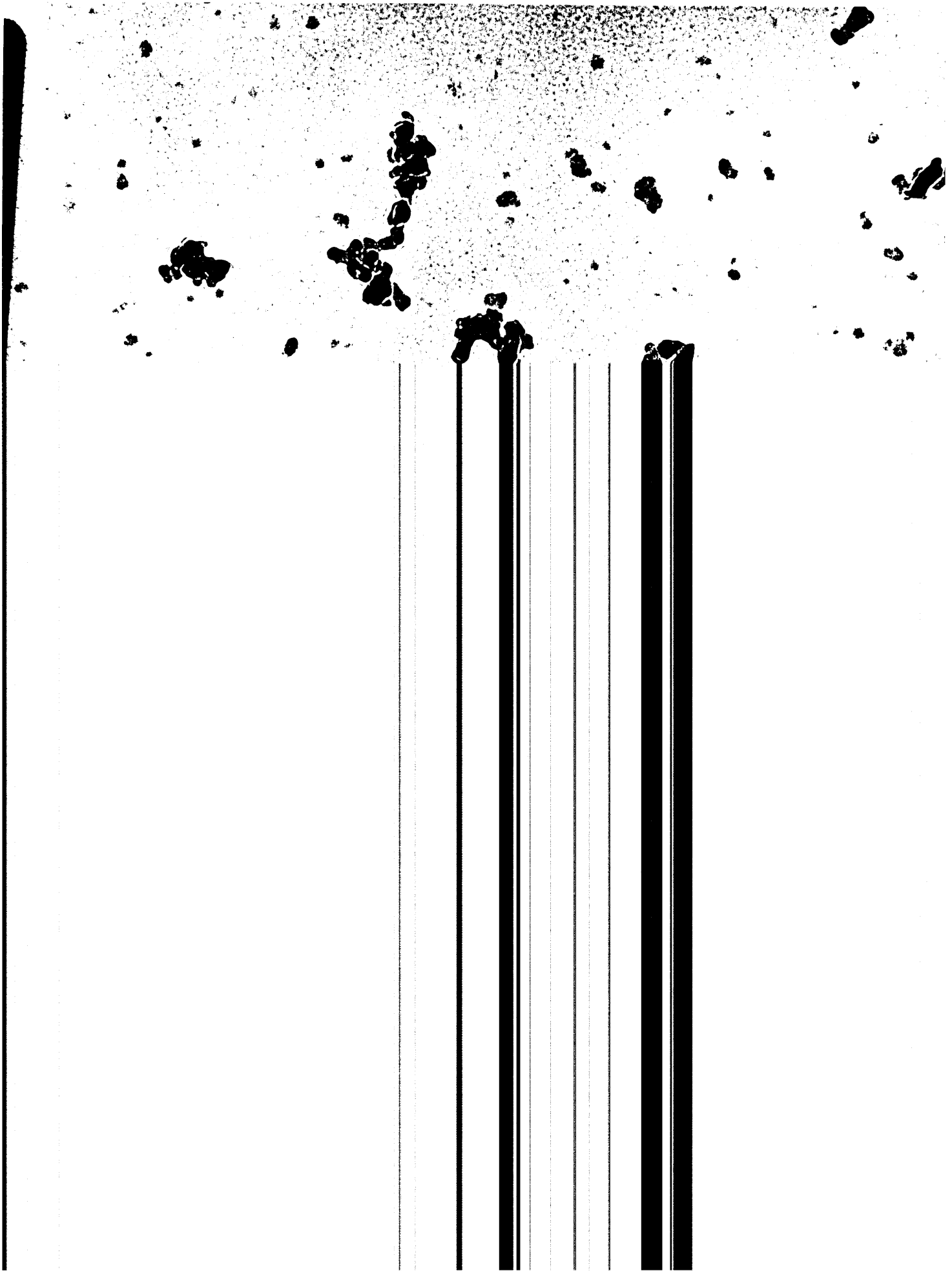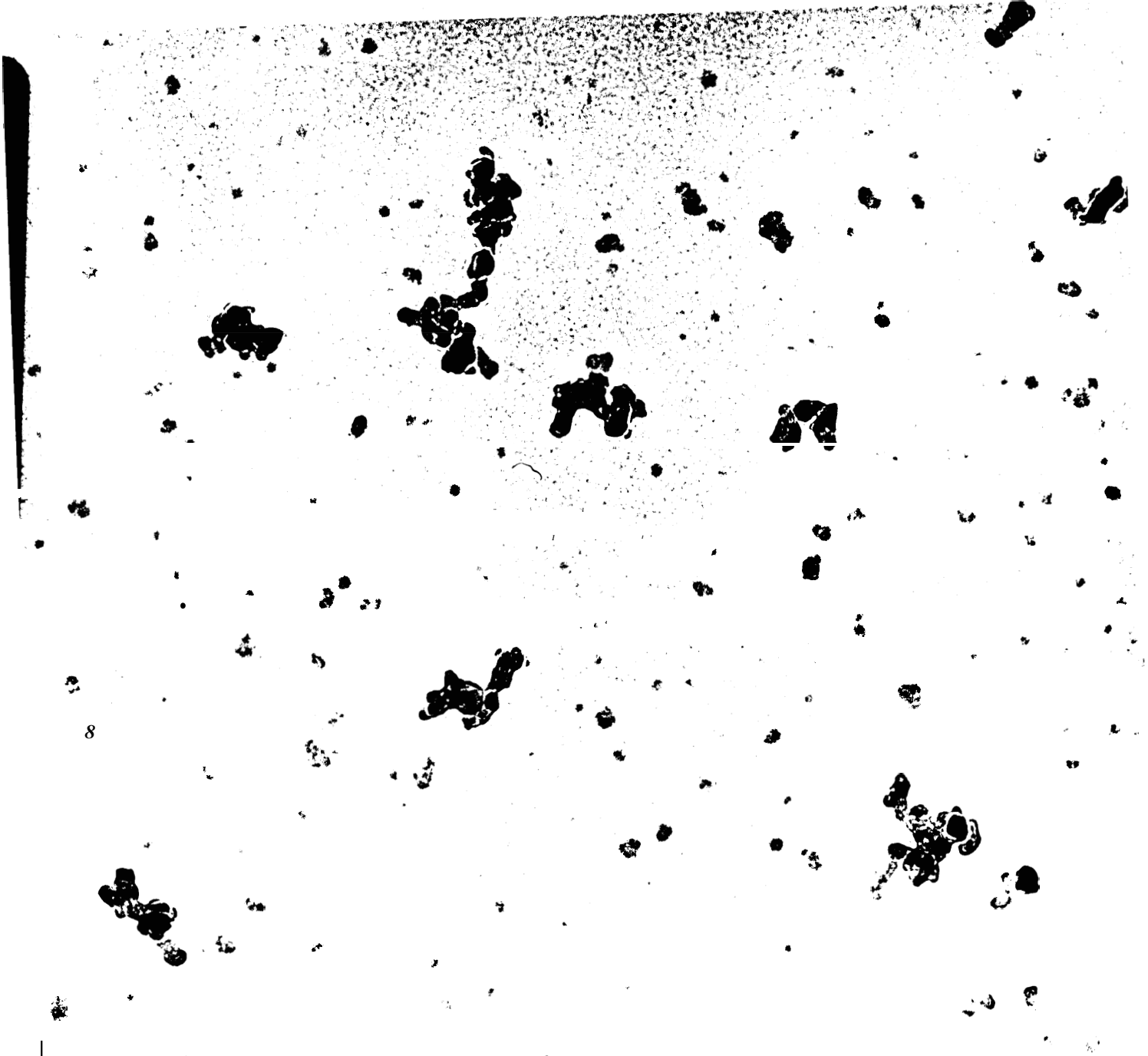
8

3

Figure 10: Soot Morphology at Z=1 cm, R=0.5 cm
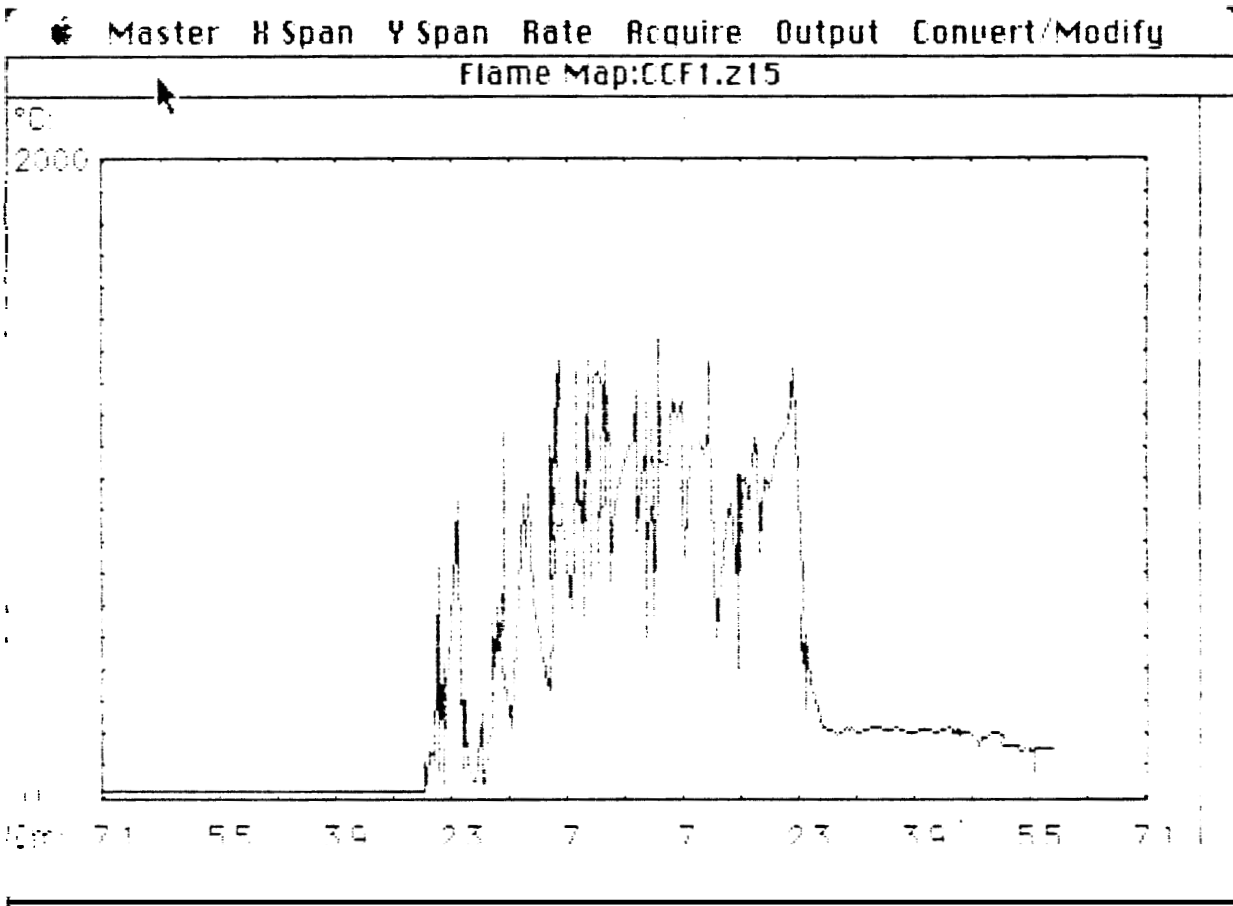
36

Figure 11: Temperature profile, **T** vs **R**, at **Z=15** cm

NIST-114A (REV. 3-90)	U.S. DEPARTMENT OF COMMERCE NATIONAL INSTITUTE OF STANDARDS AND TECHNOLOGY	1. **PUBLICATION OR** REPORT NUMBER NIST-GCR-92-609
		2. PERFORMING ORGANIZATION REPORT NUMBER
	BIBLIOGRAPHIC DATA SHEET	3. PUBLICATION DATE **July 1992**

Soot Formation in the Buoyancy-Dominated Ethene Diffusion Flame	

5. AUTHOR(S)

Haran Subramaniasivam

6. PERFORMING ORGANIZATION (IF JOINT OR OTHER THAN NIST, SEE INSTRUCTIONS) **Brown University** **Division of Engineering** **Providence, RI 02912**	7. **CONTRACT/GRANT** NUMBER Grant Nos. **60NANB9D0975 & NANB1D1110**
	8. TYPE OF REPORT AND PERIOD COVERED Thesis

10. SUPPLEMENTARY NOTES

11. ABSTRACT (A 200-WORD OR LESS FACTUAL SUMMARY OF MOST SIGNIFICANT INFORMATION. IF DOCUMENT INCLUDES A SIGNIFICANT BIBLIOGRAPHY OR LITERATURE SURVEY, MENTION IT HERE.)

A sampling technique, based on the phenomenon of thermophoresis is used here, in order to study the soot morphology within a buoyancy-dominated ethene diffusion flame. The buoyancy-dominated flame has a fuel flow rate of 50 cc/s and a co-annular air flow of 107 cc/s. Soot morphologies at each sampling location are obtained on carbon-coated grids through a fast probe drive mechanism, and they are analyzed under a transmission electron microscope. These observations, coupled with temperature measurements at various heights of the buoyancy-dominated flame, leads to a basic understanding of particle inception region, surface growth, aggregate formation, oxidation process, aggregate size and primary particle size within this flame. Change in soot morphology is studied both in the vertical and radial axes of this flame. The intense particle inception region, characterized by a large concentration of liquid-like microdroplets, is contained within the low part of the flame. These microdroplets form on the fuel side of the flame front where the temperature is the highest. Above the inception region aggregates of increasing size are observed, i.e., increasing number of primary particles, while the primary particles themselves undergo surface growth. Surface growth in primary particles ceases to exist above the vortex region of the flame, i.e., above $Z=15$ cm. Since there is very little evidence of oxidation taking place within this buoyancy-dominated flame, it is concluded that most of the soot formed in this flame is released into the surroundings. Observations being made here have been compared to similar soot morphology studies previously made on laminar ethene diffusion flames, both non-sooting and sooting, and laser diagnostic tests.

12. KEY WORDS (6 TO 12 ENTRIES; ALPHABETICAL ORDER; CAPITALIZE ONLY PROPER NAMES; AND SEPARATE KEY WORDS BY SEMICOLONS)

ethylene; diffusion flames; laminar flames; lasers; particle size; sampling; *soot*